

Davi Uliana

Homework 3 Report – Finite Element Modelling of an Aluminium Gearbox



Contents

1.	Introduction.....	3
2.	Geometry and Material Properties	4
2.1.	Geometry	4
2.2.	Material Properties of Aluminium	4
3.	Model Setup.....	4
3.1.	Preparation.....	4
3.2.	Assumptions and simplifications	5
3.3.	Non-Linear Analysis	5
4.	Mesh Optimisation	6
4.1.	Mesh Quality.....	6
5.	Results and Discussion.....	8
5.1.	Thermal-Structural analysis.....	8
5.2.	Modal and Harmonic analysis	9
5.3.	Linear Buckling analysis	10
5.4.	Non-Linear Analysis	11
5.5.	Sub-Modelling.....	14
6.	Conclusions.....	17
6.1.	Thermal-Structural Analysis.....	17
6.2.	Modal and Harmonic Analysis	17
6.3.	Linear Buckling Analysis	17
6.4.	Non-Linear Analysis	17
6.5.	Sub-Modelling.....	18

1. Introduction

This report presents a comprehensive finite element analysis (FEA) of an aluminium gearbox subjected to combined thermal and mechanical loading conditions. The objective of this study is to evaluate the structural and thermal behaviour of the gearbox under realistic service conditions using ANSYS simulation tools. The analysis includes a sequence of simulations: thermal-structural coupling, modal analysis, harmonic response, linear buckling, nonlinear elastoplastic behaviour, and sub-modelling of a critical region.

The thermal loads are defined by convective heat transfer on internal and external surfaces, while mechanical loads include bearing forces, remote directional forces, and internal pressure.

The study aims to:

1. Capture the displacement and stress distributions.
2. Identify natural frequencies and mode shapes.
3. Assess dynamic response.
4. Determine critical buckling pressure.
5. Evaluate material yielding behaviour under complex loading. A sub-modelling approach is also employed to refine stress analysis in a geometrically modified region of interest.

This report documents the methodology, modelling decisions, meshing strategy, boundary conditions, and interpretation of results, supported by visual evidence from ANSYS simulations. The goal is to demonstrate a thorough understanding of FEA principles and their application to real-world mechanical systems.

2. Geometry and Material Properties

2.1. Geometry

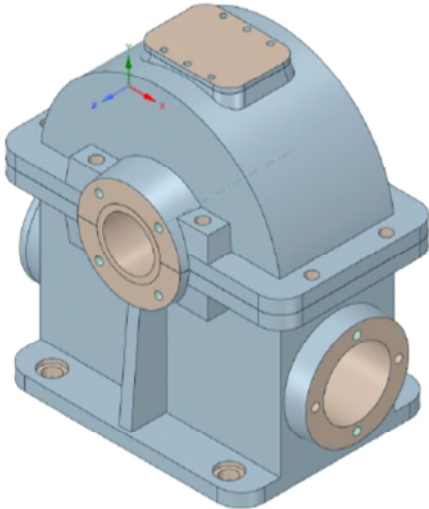


Figure 2.1.1 Gearbox Geometry

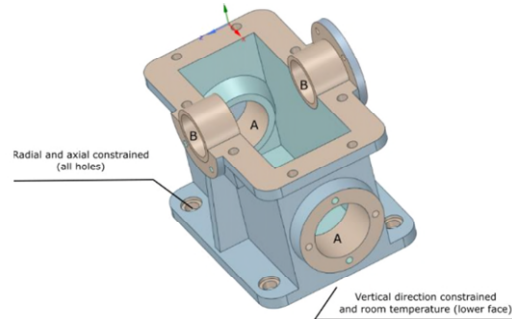


Figure 2.1.2 Geometry Constraints

2.2. Material Properties of Aluminium

Property	Value	Unit
Density	2770	Kg m ³
Young's Modulus	71	GPa
Poisson's Ratio	0.33	N/A
Tensile Yield Strength	0.28	GPa
Compressive Yield Strength	0.28	GPa
Yield Stress*	0.23	GPa
Tangent modulus*	1	GPa

*Only used for non-linear analysis.

3. Model Setup

3.1. Preparation

To improve the mesh quality, the top and bottom casing of the gearbox were subdivided into four parts as shown in Figure 3.1.1 below. Additionally, to enhance refinement in areas of high stress, the faces of the ribs beneath the front and rear Bearing B boss were also subdivided, along with the surfaces of the holes where the model is supported. This method helps to enhance the overall mesh quality.

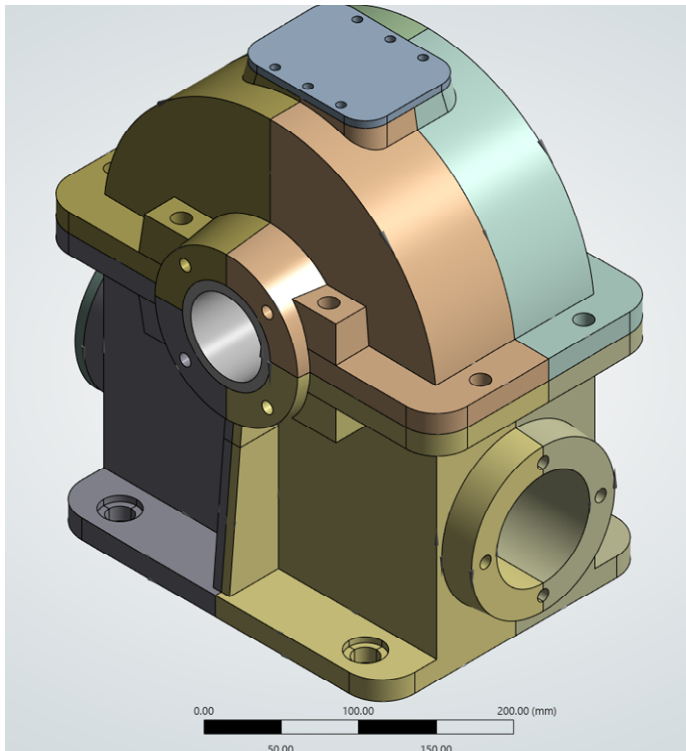


Figure 3.1.1 Gearbox Geometry Preparation

3.2. Assumptions and simplifications

1. The model is partially symmetric, so no symmetry can be assumed.
2. Bonded contacts were applied to all joints.
3. No special handling to the bolt junctions, treated faces as bonded contact.

3.3. Non-Linear Analysis

3.3.1. Full model

Additional preparation was performed for the non-linear analysis. The models were further sub-divided to enhance the mesh quality. The two ribs at the front and back of the gearbox were separated from the main body and divided into four rigid bodies each, allowing for improved control over the mesh.

3.3.2. Sub-model

A rectangular section at the back of the gearbox was cut for the sub-model, and the analysis was performed. The sub-model still included two rigid bodies.

3.3.3. Material

The material properties used for this simulation are provided in Section 2.2 of this report. All models utilized the standard Aluminium Alloy library available in Ansys Workbench, with the non-linear analysis incorporating Bilinear Isotropic Hardening properties as detailed above.

4. Mesh Optimisation

4.1. Mesh Quality

Several measures were implemented to ensure high mesh quality, including the introduction of a body size for larger models and a face size for rib faces, as well as verifying the mesh quality using element size, as shown in Figure 4.1.3. An analysis was conducted to determine the appropriate element sizes for each component. As illustrated in Figure 4.1.1 below, there is a slight increase in stress at the first two data points. However, as the element size is further reduced, stress singularities emerge, which will be addressed later in this report. Based on this analysis, it can be stated that a mesh size equivalent to design point 1 is acceptable. Please refer to the model for mode details on the element sizing.

Image Figure 4.1.4 and Figure 4.1.5 is a pictural representation of the averaged and unaveraged stresses from the same location. It should that both have similar values and thus confirming that the mesh quality is acceptable.

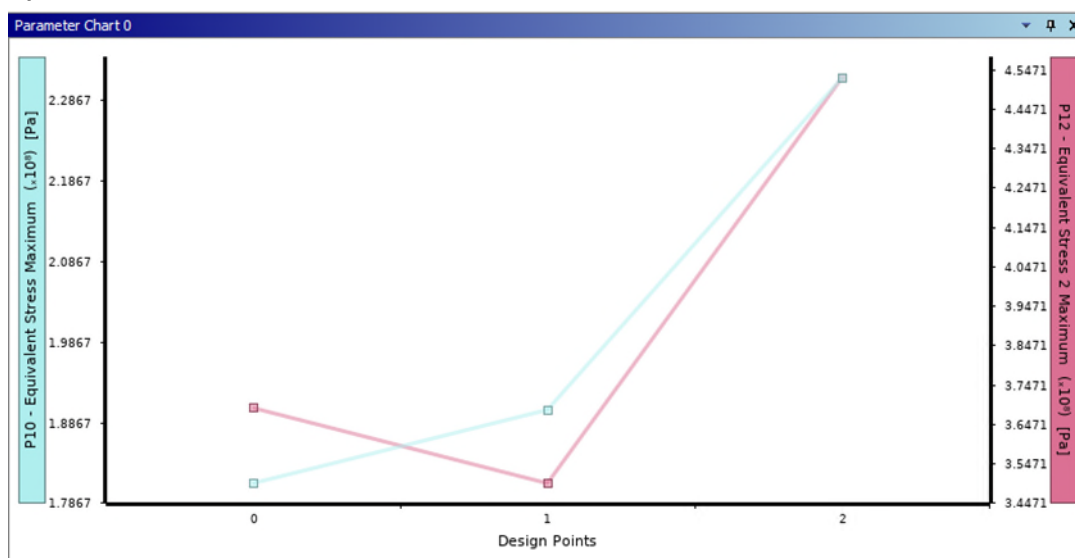


Figure 4.1.1 Averaged (left) and Unaveraged Stress comparison (right)

Homework 3 Report | Master's Degree in Numerical Simulation

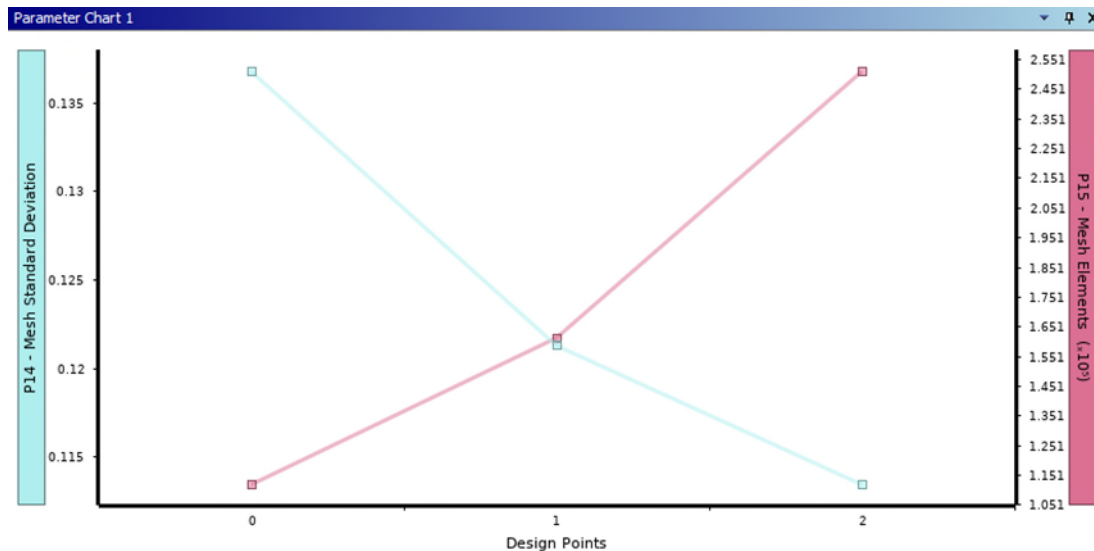


Figure 4.1.2 Element size Std Deviation (left) and Element Count (right)

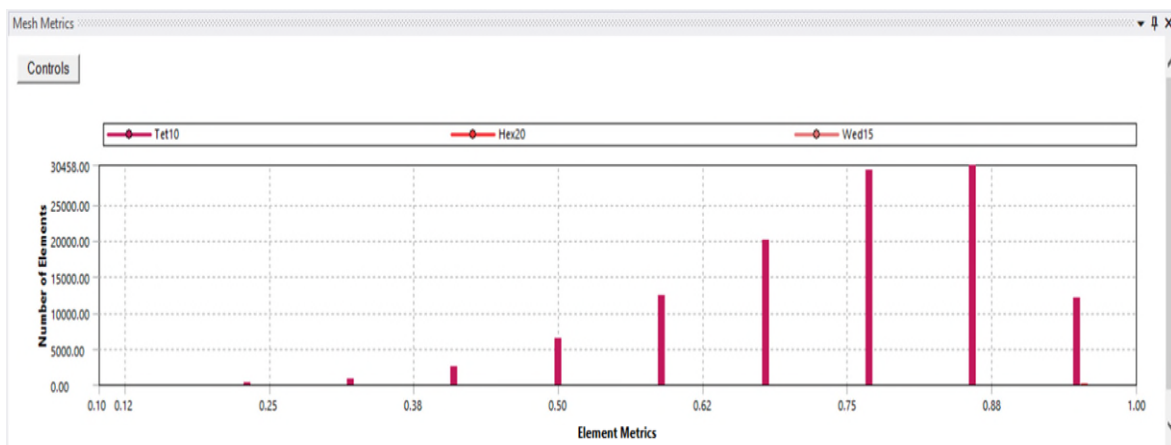


Figure 4.1.3 Mesh Quality. The image illustrates the count of element quality, with 1 indicating good quality and 0 indicating poor quality.

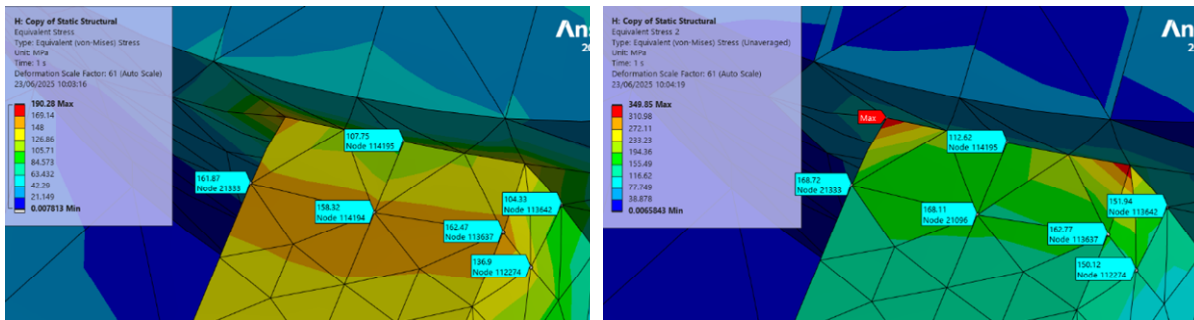


Figure 4.1.4 Averaged Von-Mises Stress. The image shows the stress values for each of the six selected nodes; from left to right: 161.87, 158.32, 107.75, 162.47, 136.9, 104.33

Figure 4.1.5 Unaveraged Von-Mises Stress. The image shows the stress values for each of the six selected nodes; from left to right: 168.72, 168.11, 112.62, 162.77, 150.12, 151.94.

5. Results and Discussion

5.1. Thermal-Structural analysis

The analysis shows that the on a linear analysis, the model can withstand its applied loads with a minimum safety factor of 0.2 around the cylindrical support locations (Figure 5.1.1). The remaining of the model has a much higher safety factor ranging from 5 to 15.

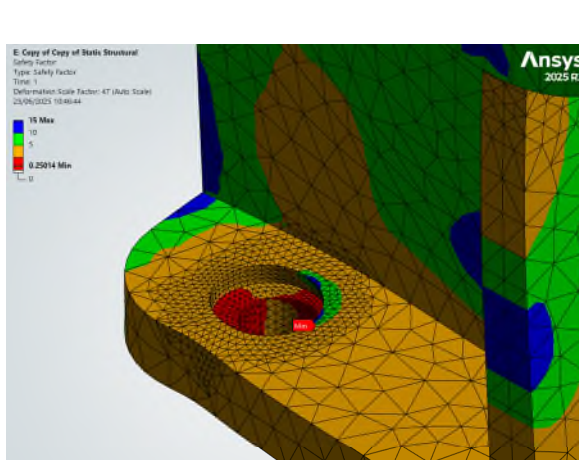


Figure 5.1.1 Safety Factor on thermal-structural analysis with 100% of thermal load and 75% of mechanical loads.

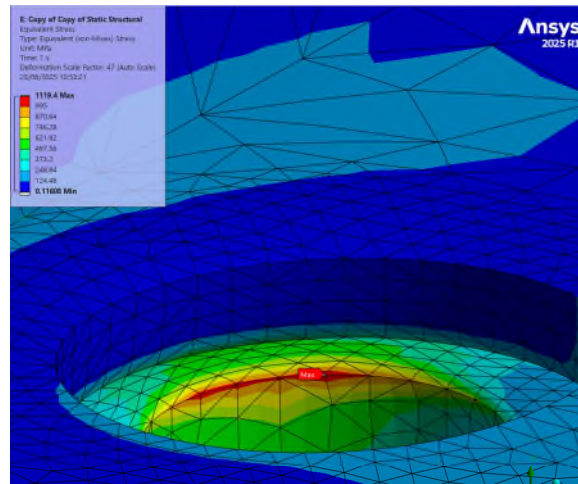


Figure 5.1.2 Von-Mises Stress thermal-structural analysis with 100% of thermal load and 75% of mechanical loads.

In accordance with the safety factor analysis, it is evident that the average von Mises stress at the same location exhibits a very high stress value as shown by Figure 5.1.2 above, suggesting the presence of stress concentration or singularity at the edge of the hole. Additionally, the fact that the stress within the same element ranges from 1120 MPa to below 500 MPa further indicates the possibility of a stress singularity.

It is recommended to create a sub-model of this region to investigate the actual stresses experienced by the model in greater detail. Alternatively, refining the mesh in this region could be considered; however, this approach would be more computationally expensive and may potentially accentuate the stress singularity.

5.2. Modal and Harmonic analysis

The modal response analysis indicates that the point of resonance occurs at approximately 1050Hz. The graph shown in Figure 5.2.1 below compares the frequency response across all three axes. It is observed that the x-axis has the highest amplitude, leading to the conclusion that the harmonic response occurs around 1050Hz in the X-axis direction.

This phenomenon is further elucidated by comparing the phase response angle across different frequencies around the resonance point, as illustrated in Figure 5.2.2 below. The stress reaches its maximum at 1050 Hz, with a value of 12.5 MPa (Figure 5.2.4), which is notably higher than other frequencies that range from 0.5 to 5.5 MPa.

We see that the input and output values are symmetrical, confirming a steady-state harmonic response as shown in Figure 5.2.3.

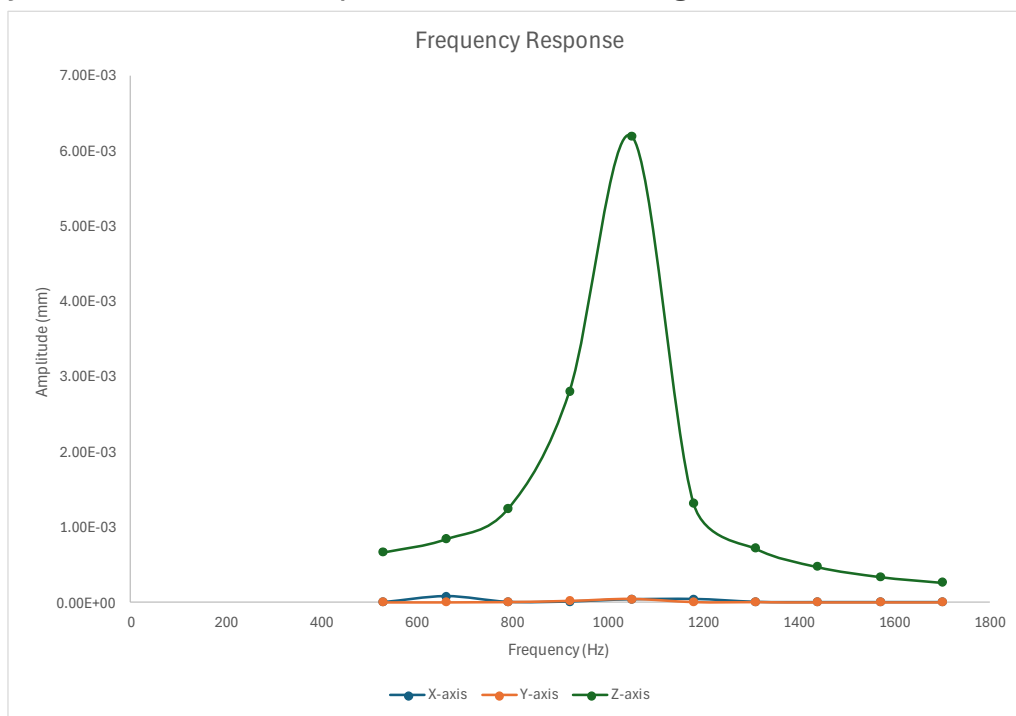


Figure 5.2.1 Frequency Response. X, Y and Z-axis.

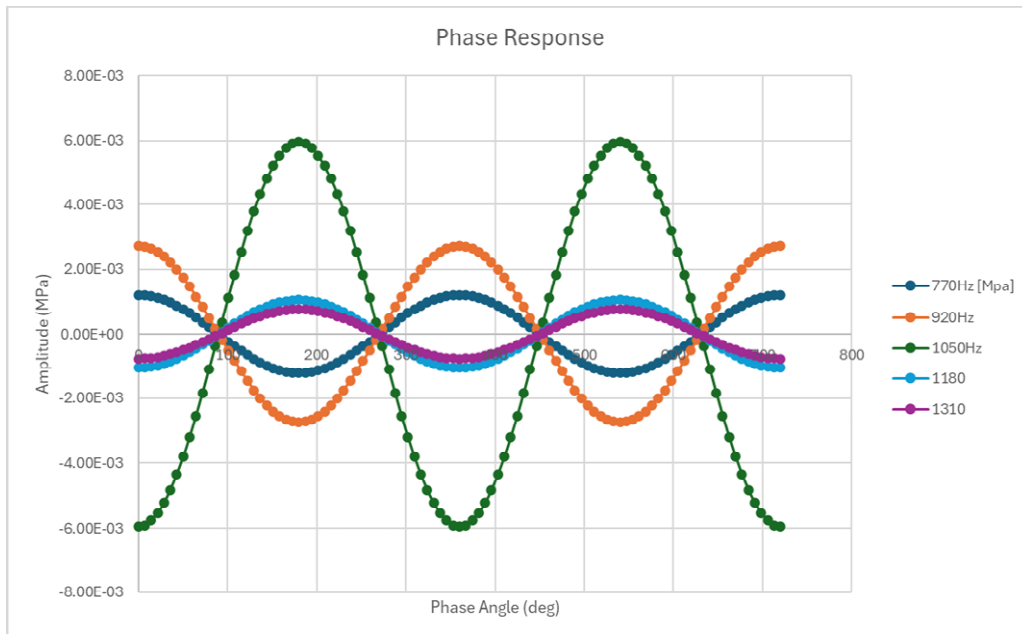


Figure 5.2.2 Phase Response Angle

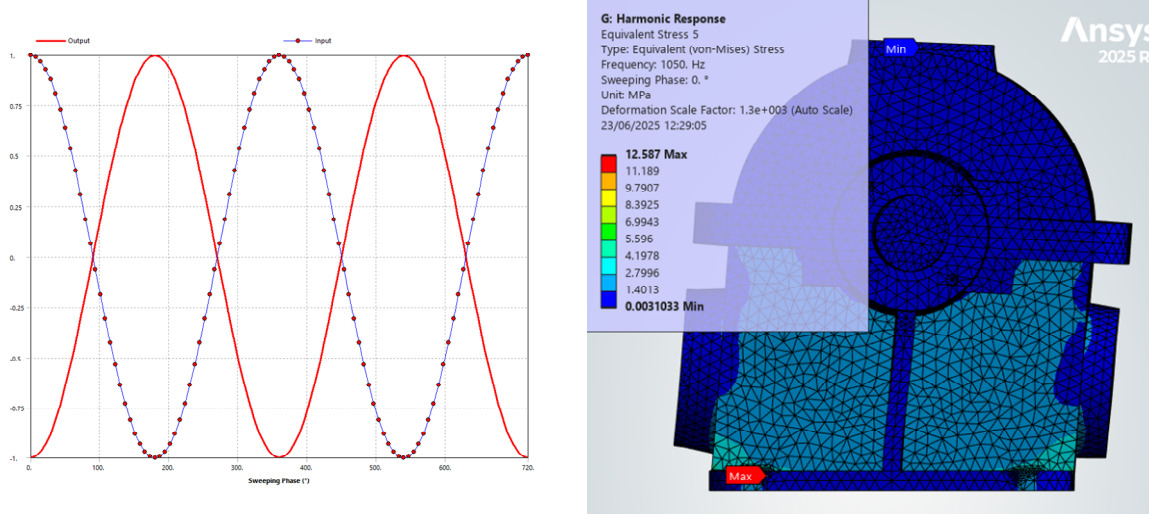


Figure 5.2.3 Phase Response Graph for 1050Hz showing the symmetry of both input and output confirming steady-state harmonic response.

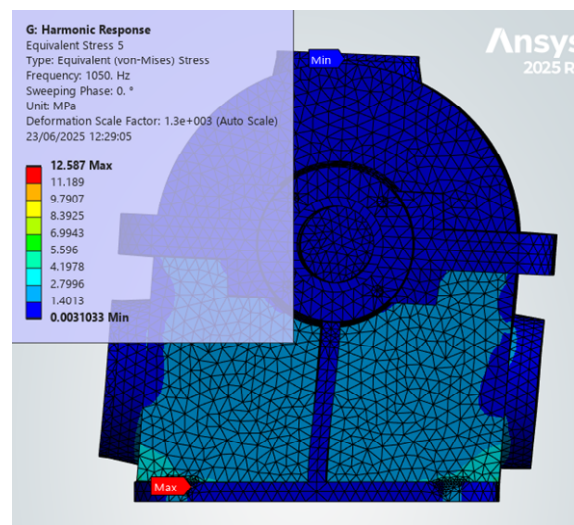


Figure 5.2.4 Harmonic response with plotted deformation and stress.

5.3. Linear Buckling analysis

The critical buckling analysis indicated that for the first two modes of buckling, the load multiplier is negative. This suggests that buckling would occur in the direction opposite to the applied load, which in this case is a positive internal pressure. However, for this specific example, we are

interested in the critical buckling behaviour when the model is subjected to an internal negative pressure. Therefore, the analysis settings were adjusted to consider only positive values.

The most critical load multiplier is the first mode. However, the load is very large which confirms that the assembly is stable at the applied pressure.

Because:

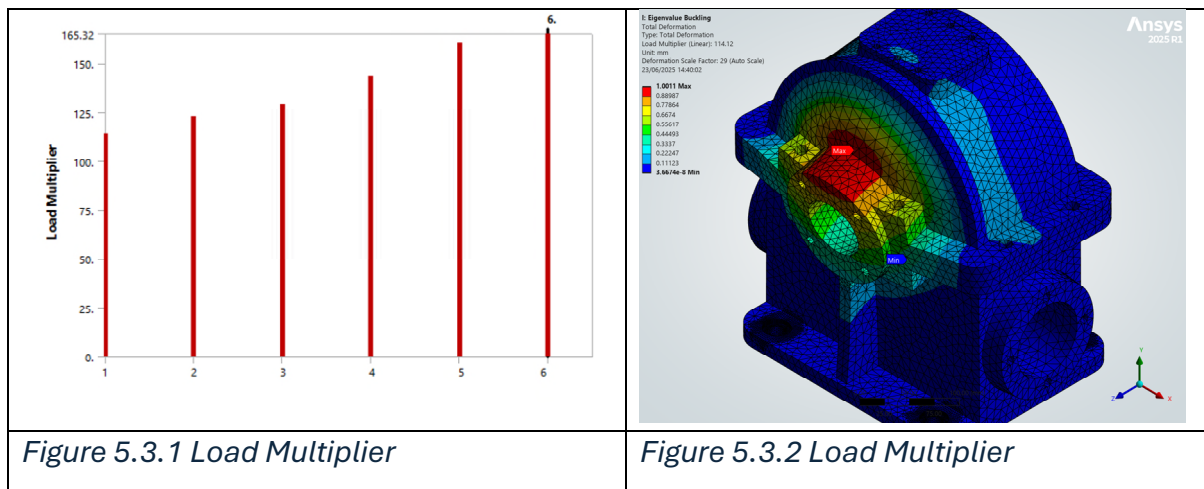
$$F_{buckle} = (F_{applied} \times \lambda_i)$$

Hence:

$$F_b = -3Mpa \times 114.12$$

$$F_b = -342.36MPa$$

Which means that the structure has > 100 times safety factor for applied load of (-3MPa)



5.4. Non-Linear Analysis

5.4.1. Settings

According to the problem description and as seen on Figure 5.4.1, the analysis comprised 15 steps, with sub-steps managed programmatically rather than manually.

Non-linear control settings included Line Search to enhance convergence and Stabilization turned OFF.

Output control settings were configured as follows: Stress, strain, and General Miscellaneous set to ON, with results stored at all time points.

Restart controls were set to Manual, ensuring that all steps were loaded.

5.4.2. Results

The analysis shows good mesh convergency with element quality concentrating between 0.7 and 0.9 (see Figure 5.4.5 below) and the averaged and unaveraged (Figure 5.4.3 and Figure 5.4.4) von-mises showing very similar results (495MPa).

However, as seen previously this is a spot of high stress concentration and to obtain a more accurate reading a sub-modelling is recommended.

The model successfully obtained convergence as seen on Figure 5.4.6. from observing the Stress and Strain plots we can see the load



Figure 5.4.1 Settings

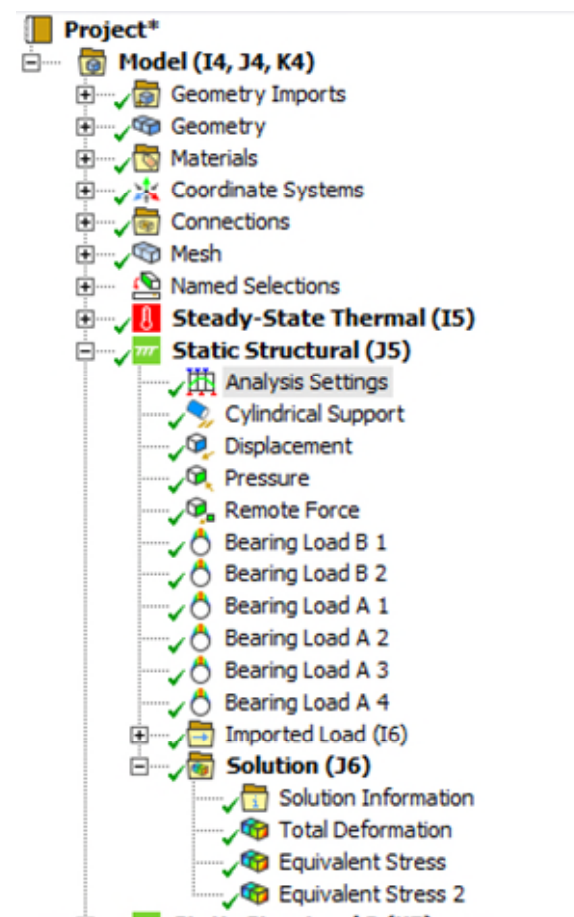


Figure 5.4.2 Model Tree

Homework 3 Report | Master's Degree in Numerical Simulation

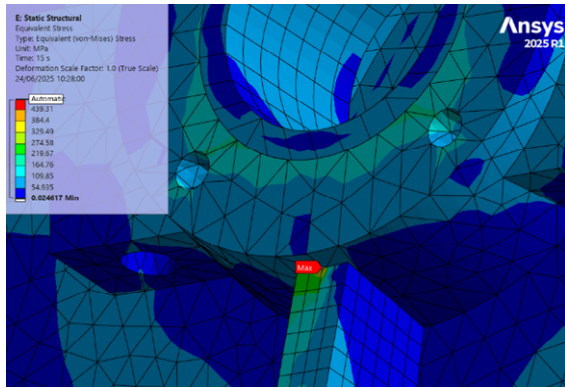


Figure 5.4.3 Averaged Von-Mises

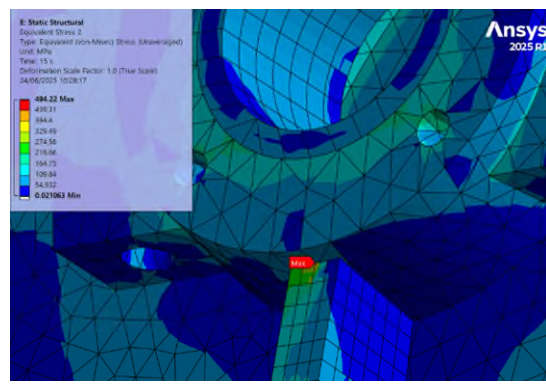


Figure 5.4.4 Unaveraged Von-Mises

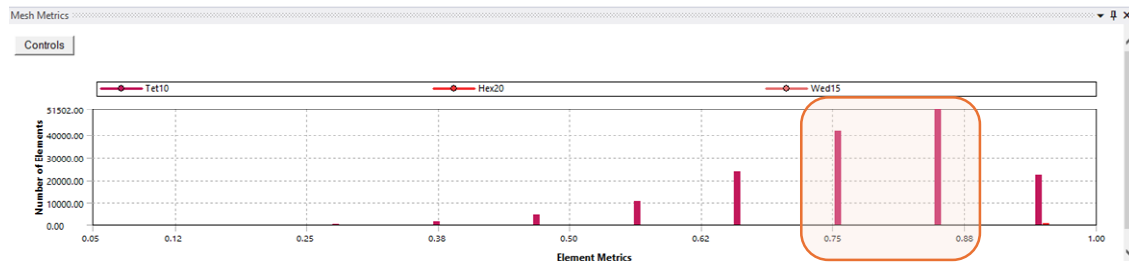


Figure 5.4.5 Element Quality

The force convergence plot in Figure 5.4.6 below demonstrates that all steps have converged appropriately. The Stress curve shown in Figure 5.4.7 indicates two limit points at step 1 and 7.4, which corresponds to the Force Convergence graph. Here, the initial step is loaded quickly, followed by smaller steps until full convergence is achieved.

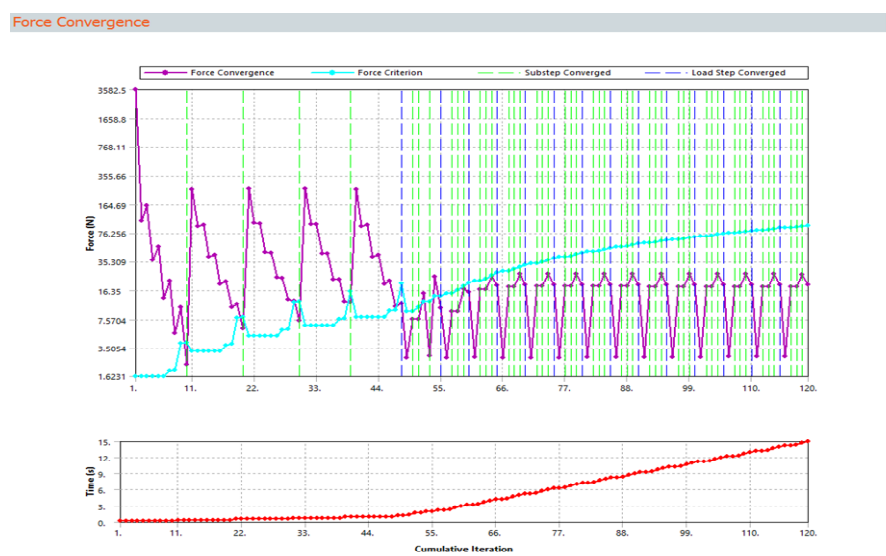


Figure 5.4.6 Force Convergence Plot

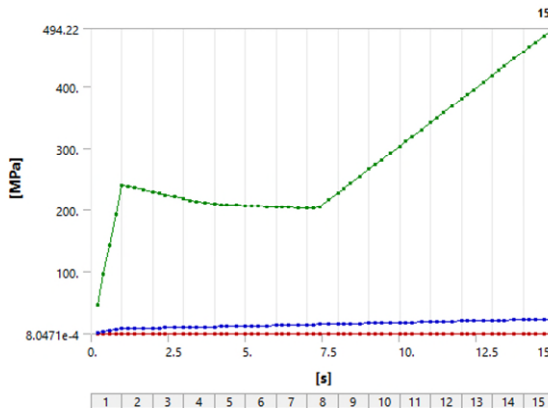


Figure 5.4.7 Stress and Strain vs Time

5.5. Sub-Modelling

The sub-model incorporated a rectangular section at the back rib where stress peaked during the non-linear analysis. The refined mesh and reduced model size facilitate a swift solution and provide a more precise reading of the stress concentration. Furthermore, radii were added to the model to enhance realism and support the stress concentration.

Only internal pressure was applied; other loads are included in the “Cut Boundary Constraint”.

To verify the cut boundary mapping, a line geometry and "Linearized Stress" were introduced. Figure 5.5.3 and Figure 5.5.4 show that the linearized stress matches, indicating a well-defined sub-model cut boundary.

Having established that the model is in agreement, it is now possible to interpret the results of the sub-model simulation. The Force Convergence graph (Figure 5.5.5) indicates that all steps converged successfully. However, we still observe areas of high stress concentration. The element quality indicates we should have a good mesh, but the averaged and unaveraged stresses as well as the structural error (Figure 5.5.7) indicates that we need further improvement.

Homework 3 Report | Master's Degree in Numerical Simulation

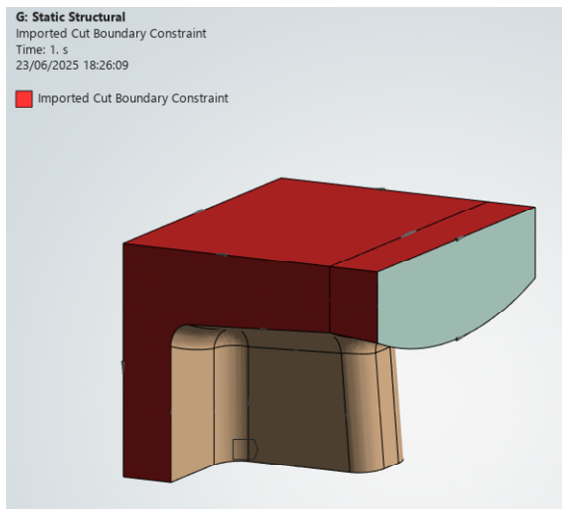


Figure 5.5.1 Sub-Model Geometry

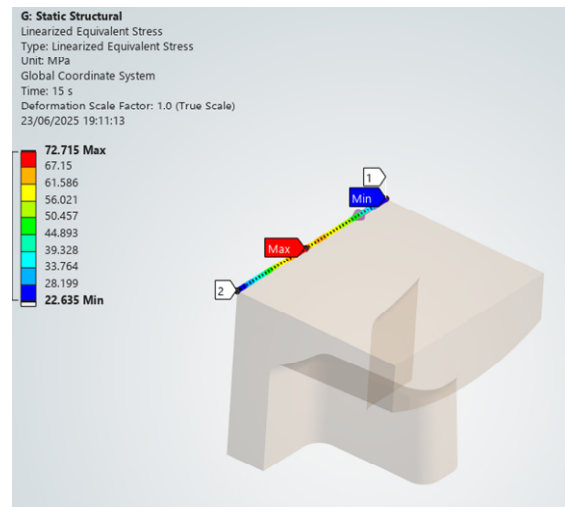


Figure 5.5.2 Sub-Model Cut Boundary Verification Plot

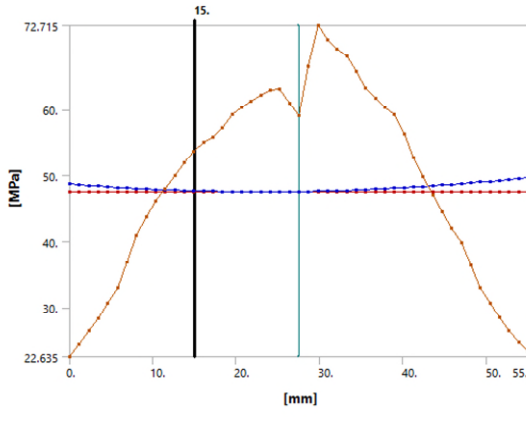


Figure 5.5.3 Sub-Model Cut Boundary Verification

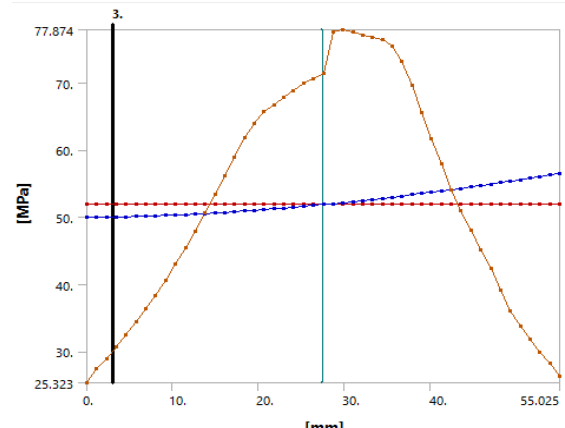


Figure 5.5.4 Full Model Cut Boundary Verification

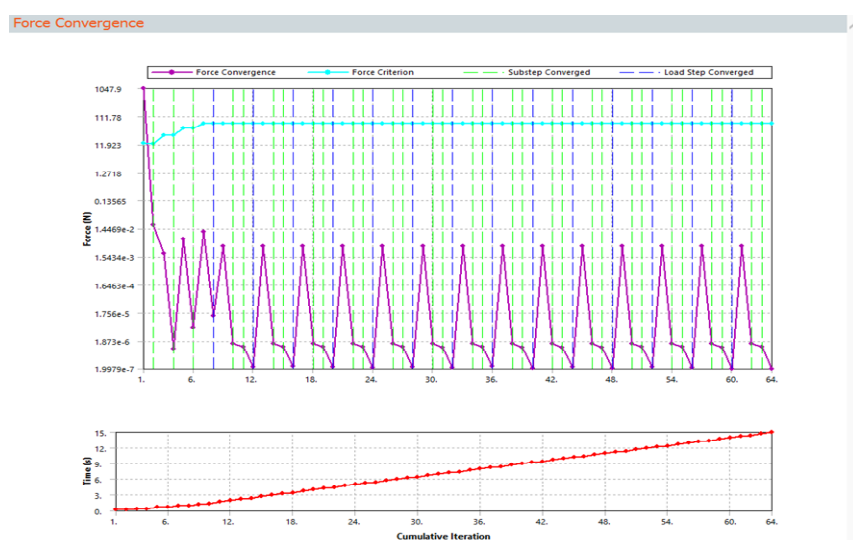
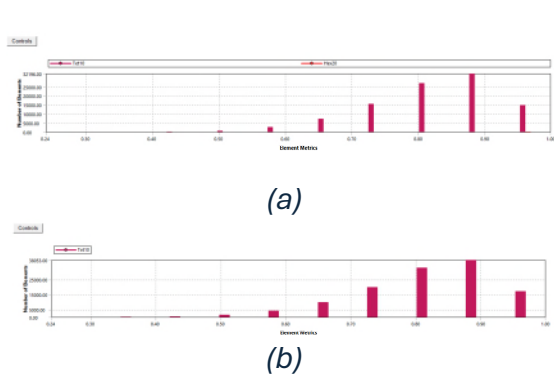


Figure 5.5.5 Sub-Model Force Convergence

Homework 3 Report | Master's Degree in Numerical Simulation



*Figure 5.5.6 Sub-Model Element Quality
(a) pre refinement; (b) post refinement*

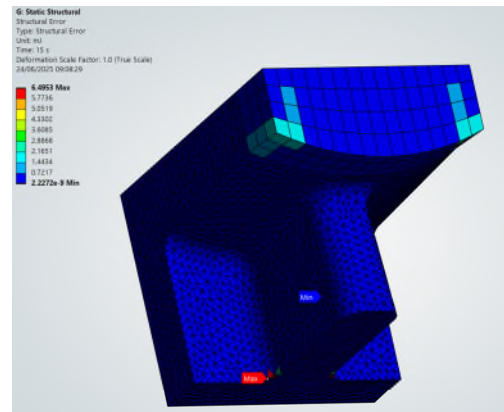


Figure 5.5.7 Structural Error

After rerunning the analysis with the improved mesh, it was observed that the maximum stress reached over 2000MPa at the edge of the cut boundary. This indicates that the structural error observed earlier is not due to poor mesh quality. Additionally, by applying two ranges on the stress contour plot ranging from 0-230MPa and 230->Max (as seen in Figure 5.5.8below), it can be noted that the stresses in the radii region peak at 230MPa. This is lower than the stress range observed in the full model (without radii), which peaks at 281MPa.

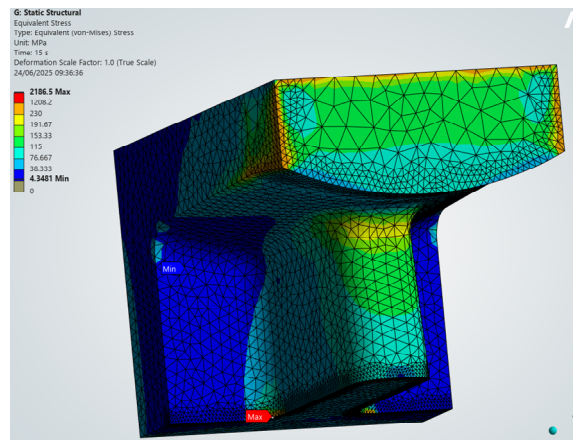


Figure 5.5.8 Sub-Model Stress Plot. The plot shows the stress contour on the sub-model with a range set on the scale between 0-230MPa (yellow).

6. Conclusions

6.1. Thermal-Structural Analysis

The linear thermal-structural analysis revealed that while the majority of the model maintains a high safety factor (ranging from 5 to 15), critical stress concentrations exist near the cylindrical support regions, where the safety factor drops to 0.2. This suggests potential stress singularities, likely due to geometric discontinuities such as holes. Further investigation through sub-modelling or mesh refinement is recommended to accurately assess the stress distribution in these critical areas.

6.2. Modal and Harmonic Analysis

The modal analysis identified a resonance frequency at approximately 1050 Hz, with the X-axis exhibiting the highest amplitude response. The harmonic analysis confirmed a steady-state response at this frequency, with peak stress reaching 12.5 MPa. These findings highlight the importance of considering dynamic loading conditions in the design, particularly in the X-direction.

6.3. Linear Buckling Analysis

The buckling analysis demonstrated that the structure is highly stable under the applied internal pressure, with a critical load multiplier of 114.12. This corresponds to a buckling load of -342.36 MPa, indicating a safety factor exceeding 100. The negative load multipliers in the first two modes suggest buckling in the opposite direction of the applied load, which aligns with the analysis focus on internal negative pressure.

6.4. Non-Linear Analysis

The non-linear analysis confirmed good mesh quality and convergence, with von Mises stress values around 495 MPa in high-stress regions. However, due to the presence of stress concentrations, sub-modelling was necessary to obtain more accurate results. The analysis also revealed two limit points in the stress-strain response, indicating non-linear behaviour under loading.

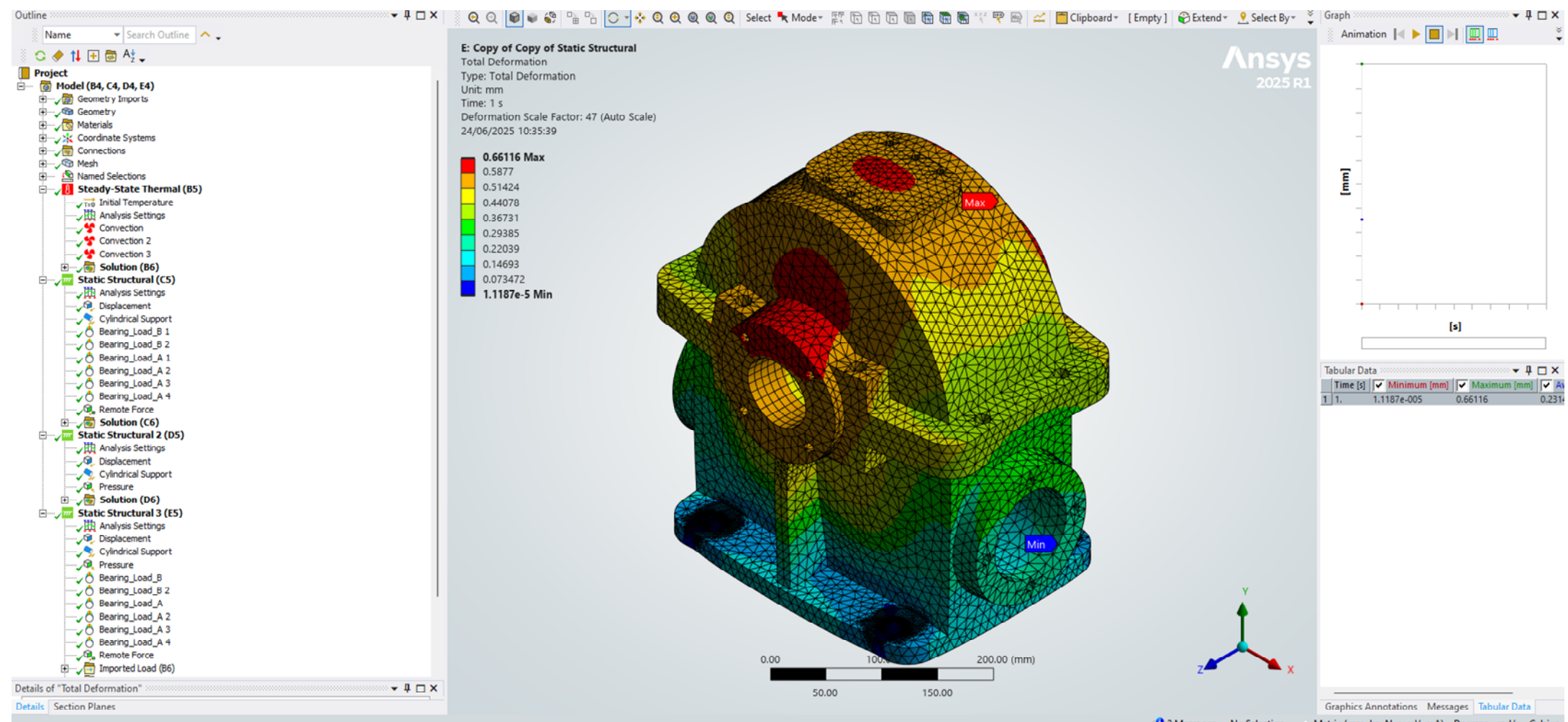
6.5. Sub-Modelling

Sub-modelling of the high-stress region provided a more refined understanding of local stress behaviour. The improved mesh and added radii reduced peak stress from 281 MPa (in the full model) to 230 MPa. However, extremely high stress values (>2000 MPa) were still observed at the cut boundary, suggesting that further refinement or design modifications may be necessary to mitigate these concentrations.

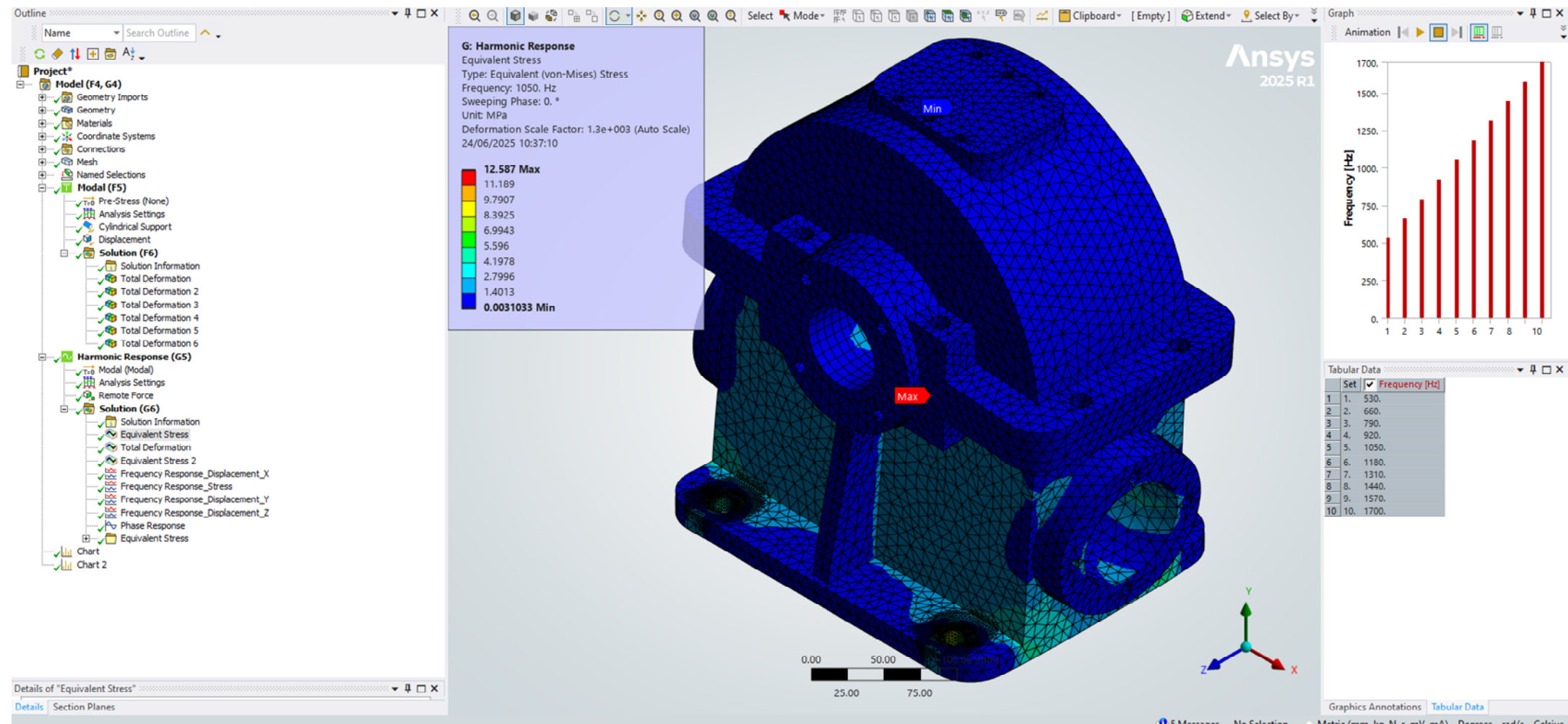
Bibliography (Harvard Style)

Enterfea. (n.d.). *Linear buckling in plain language!*. [online] Available at: <https://enterfea.com/linear-buckling-explained/> [Accessed 24 Jun. 2025].

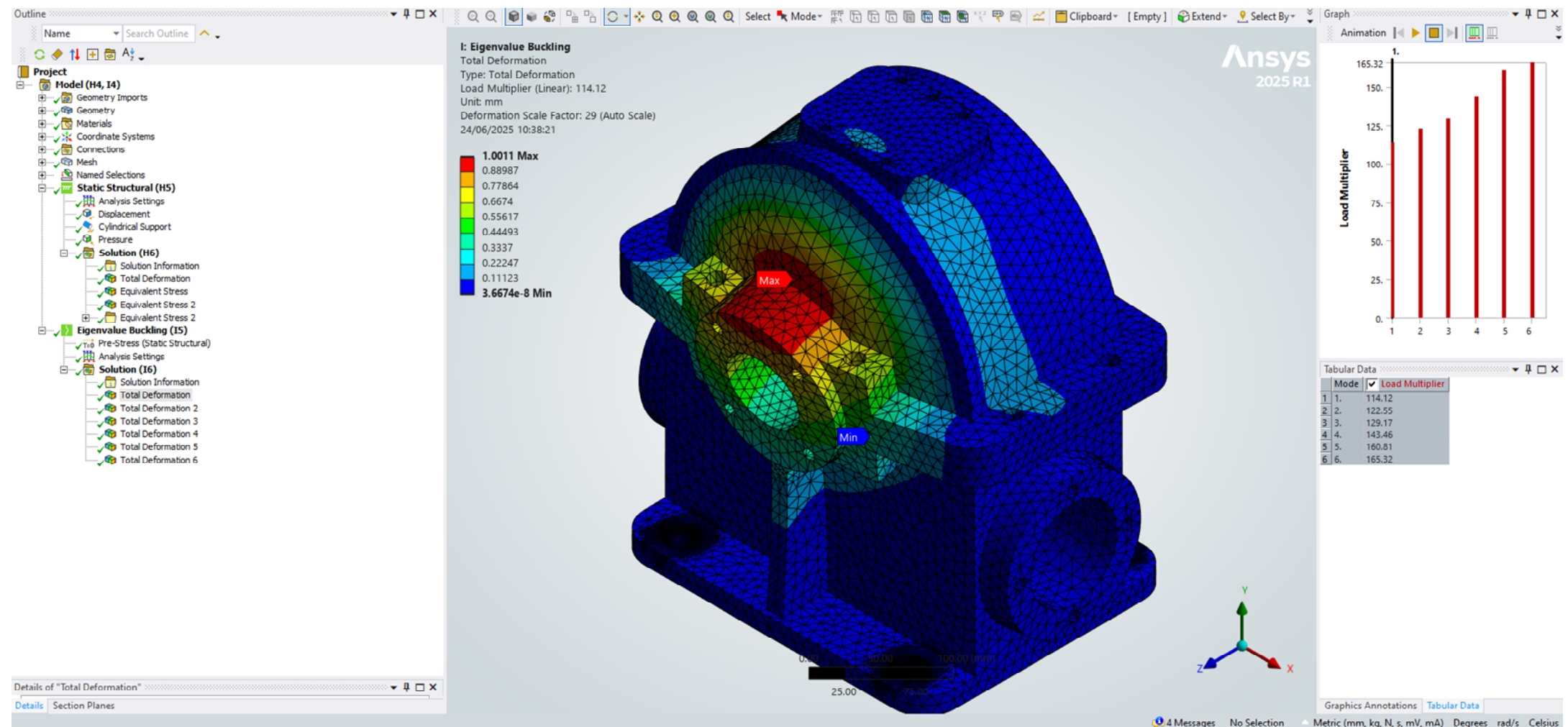
Appendix A Thermal-Structural



Appendix B Modal Harmonic

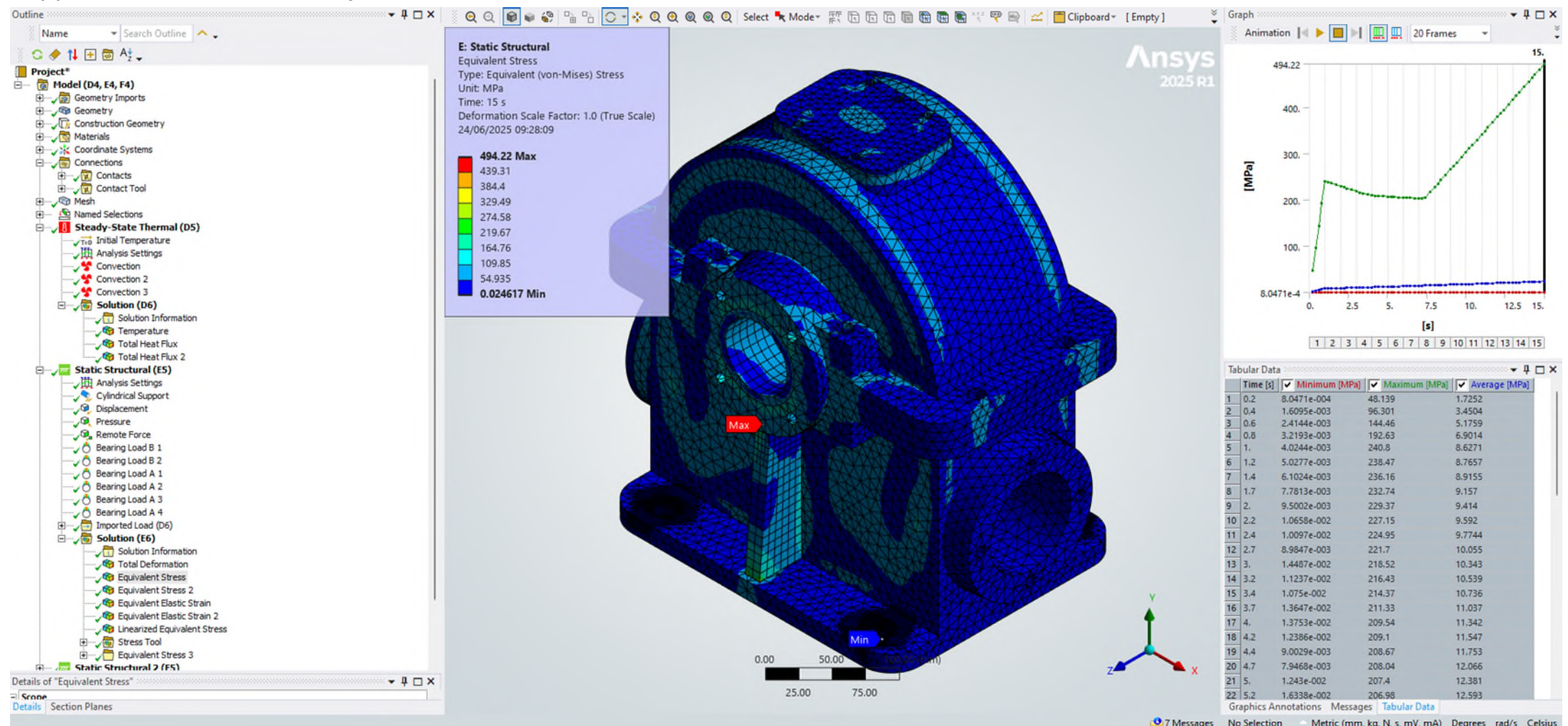


Appendix C Buckling



Uliana, Davi | 22

Appendix C Non-Linear Analyses



Uliana, Davi | 23

Appendix D Sub-Model Analysis

